Journal for ImmunoTherapy of Cancer

Trojan-horse silk fibroin nanocarriers loaded with a re-call antigen to redirect immunity against cancer

Elia Bari ,[1] Francesca Ferrera,[2] Tiziana Altosole,[2] Sara Perteghella,[3,4] Pierluigi Mauri,[5] Rossana Rossi,[5] Giulia Passignani,[5] Luca Mastracci,[6,7] Martina Galati,[2] Giuseppina Iliana Astone ,[2] Maddalena Mastrogiacomo,[2] Patrizio Castagnola,[8] Daniela Fenoglio,[2,8] Dario Di Silvestre,[5] Maria Luisa Torre ,[1,4] Gilberto Filaci [2,8]

To cite: Bari E, Ferrera F, Altosole T, *et al*. Trojan-horse silk fibroin nanocarriers loaded with a re-call antigen to redirect immunity against cancer. *Journal for ImmunoTherapy of Cancer* 2023;**11**:e005916. doi:10.1136/jitc-2022-005916

► Additional supplemental material is published online only. To view, please visit the journal online (http://dx.doi.org/10.1136/jitc-2022-005916).

EB, FF and TA contributed equally.
DDS, MLT and GF contributed equally.

Accepted 23 December 2022

For numbered affiliations see end of article.

Correspondence to
Professor Gilberto Filaci; gfilaci@unige.it

ABSTRACT

Background The current challenge for immunotherapies is to generate effective antitumor immunity. Since tumor immune escape mechanisms do not impact pre-existing and consolidated immune responses, we tested the hypothesis of redirecting a pregenerated immunity to cancer: to recall a non-tumor antigen response against the tumor, silk fibroin nanoparticles (SFNs) have been selected as 'Trojan-horse' carriers, promoting the antigen uptake by the tumor cells.

Methods SFNs have been loaded with either ovalbumin (OVA) or CpG oligonucleotide (CpG) as antigen or adjuvant, respectively. In vitro uptake of SFNs by tumor (B16/F10 melanoma and MB49 bladder cancer) or dendritic cells, as well as the presence of OVA-specific T cells in splenic and tumor-infiltrating lymphocytes, were assessed by cytometric analyses. Proof-of-concept of in vivo efficacy was achieved in an OVA-hyperimmune B16/F10 murine melanoma model: SFNs-OVA or SFNs-CpG were injected, separately or in association, into the subcutaneous peritumoral area. Cancer dimensions/survival time were monitored, while, at the molecular level, system biology approaches based on graph theory and experimental proteomic data were performed.

Results SFNs were efficiently in vitro uptaken by cancer and dendritic cells. In vivo peritumor administration of SFNs-OVA redirected OVA-specific cytotoxic T cells intratumorally. Proteomics and systems biology showed that peritumoral treatment with either SFNs-OVA or SFNs-CpG dramatically modified tumor microenvironment with respect to the control (CTR), mainly involving functional modules and hubs related to angiogenesis, inflammatory mediators, immune function, T complex and serpins expression, redox homeostasis, and energetic metabolism. Both SFNs-OVA and SFNs-CpG significantly delayed melanoma growth/survival time, and their effect was additive.

Conclusions Both SFNs-OVA and SFNs-CpG induce effective anticancer response through complementary mechanisms and show the efficacy of an innovative active immunotherapy approach based on the redirection of pre-existing immunity against cancer cells. This approach could be universally applied for solid cancer treatments if translated into the clinic using re-call antigens of childhood vaccination.

WHAT IS ALREADY KNOWN ON THIS TOPIC

⇒ The current challenge for cancer vaccines is to generate effective immune responses against cancer, overcoming the several cancer immune escape mechanisms that hamper tumor antigen-directed immune responses.

WHAT THIS STUDY ADDS

⇒ Our innovative approach redirects an already existing, robust, consolidated immune response against cancer. It exploits a 'Trojan-horse' strategy using silk fibroin nanoparticles as a vehicle of both an antigen and an adjuvant within the tumor.

HOW THIS STUDY MIGHT AFFECT RESEARCH, PRACTICE OR POLICY

⇒ This strategy, translated into clinics, could be universally applied to any cancer and any patient, using, as the immunogen, a re-call antigen: possible objectives consist both in eradication (i.e., in non-metastatic tumors like glioblastoma) and palliation (i.e., treatment of surgically unresectable tumor masses of any nature).

INTRODUCTION

Cancer vaccines should induce effector cancer-specific immune responses. However, although several cancer vaccines have been generated and tested in clinical trials, their general clinical efficacy rate was very poor,[1] and only one cancer vaccine, sipuleucel-T, received approval for clinical use.[2] The main reasons for the failure of vaccination strategy in cancer treatment are the low immunogenicity of tumor-associated antigens and the tumor capacity to downregulate their expression and generate a tolerogenic tumor microenvironment (TME).[3] Cancer vaccines based on tumor neoantigens originating from tumor-specific gene mutations[4] present some drawbacks since they are generally not shared among patients and are poorly presented

by (human leukocyte antigen) HLA molecules.[5] Moreover, they require complex and expensive technologies that dramatically impact therapy costs. Hence, there is an urgent need to imagine new approaches of cancer vaccination to overcome the current difficulties. Clinical evidence teaches that tumor immune suppression does not significantly impact pre-existing, consolidated immune responses, like those induced early in life by pediatric vaccinations.[6] Hence, a new perspective for cancer vaccination could be redirecting pre-existing immunity against tumor. This innovative strategy requires a vector able to vehicle the antigen target of the pre-existing immunity within tumor cells in association with a potent adjuvant able to subvert the immune suppressive milieu present in TME.

In this regard, nanoparticles are a promising tool in cancer immunotherapy.[7 8] They allow optimal delivery of antigens and adjuvants in TME. They may accumulate passively due to the enhanced permeability and retention effect or through specific active targeting.[9] In addition, the fact that nanoparticles may be internalized by both tumor cells and dendritic cells (DCs) allows the delivery of antigens in both cell types, thus facilitating the onset and development of an immune response. In particular, silk fibroin (SF) nanoparticles are of great interest since they are biocompatible, biodegradable, and have adequate mechanical properties for stable delivery and optimal in situ retention of drugs or antigens.[10–12]

Based on the above, we explored the efficacy of a 'Trojan-horse' model of cancer immunotherapy to recall a pre-existing immunity toward the tumor. To this aim, we used silk fibroin nanoparticles (SFNs) as a vehicle for both the antigen, ovalbumin (OVA), and the adjuvant, CpG, in OVA pre-immunized mice. Injectable formulations of SFNs loaded with OVA or CpG were designed, their in vitro internalization by cancer and DCs was determined, and their protecting efficacy against tumor growth was evaluated in a murine model. Application of high-throughput proteomics and systems biology approaches based on protein–protein interaction (PPI) network models[13] allowed the definition of functional modules and hubs involved in their activity.

MATERIALS AND METHODS

Preparation of injectable formulations of SFNs

SF was extracted and solubilized according to a previously reported procedure described in the online supplemental material. SFNs were then prepared by exploiting the fibroin desolvation in acetone.[10 12] Briefly, for SFNs preparation, SF (1.5% w/v) was added dropwise to acetone; for SFNs-OVA, a solution of SF (1% w/v) and OVA (Merck, Darmstadt, Germany) (0.5% w/v) was prepared and then added dropwise to acetone; for SFNs-CpG, a solution of SF (1.5% w/v) and CpG (TIB Molbiol, Genoa, Italy) (0.1% w/v) was prepared and then added dropwise to acetone. The fibroin/acetone volume ratio was 1:5 in all cases. The nanoparticle suspension was further processed and freeze-dried as reported in the online supplemental material. Final formulations were stored at 4°C until use (maximum of 3 months). In addition, a physical mixture of SFNs-OVA and SFNs-CpG was prepared by mixing the freeze-dried formulations of SFNs-OVA and SFNs-CpG in a 1:1 ratio.

Characterization of SFNs injectable formulations

As reported in the online supplemental material, OVA loading in SFNs-OVA was evaluated by size exclusion chromatography, quantifying the residual presence of unbound OVA in the washed supernatants.

Loading of CpG into SFNs-CpG was verified by analyzing the nanoparticles' micro-analytical composition by a high-resolution scanning electron microscopy (TESCAN, Mira 3 XMU) equipped with an In-Beam SE detector operating at 8 kV and by energy dispersive spectrometry operating at 20 kV. Before the analysis, the samples were coated with carbon using a Cressington 208C.

The dimensional distribution of SFNs was analyzed using NanoSight NS300 equipment (Malvern Panalytical, Great Malvern, Worcestershire, UK); the mean size, polydispersity index (PDI) and zeta potential were analyzed by Zetasizer Nano Zs (Malvern Panalytical) (see online supplemental material). Chemical-physical characterization was performed by recording Mid-infrared (IR) (650–4000 cm^{-1}) spectra on powder samples using a Bruker Equinox 55 spectrometer equipped with a pyroelectric detector (deuterated-triglycine-sulfate (DTGS) type) with a resolution of 4 cm^{-1}. Following the procedures reported in the online supplemental material, temperature and enthalpy values were measured by differential scanning calorimetry (DSC) by a NEXTA DSC (Hitachi, Europark Fichtenhain A12, Krefeld, Germany) equipped with a DSC821e module and an intracooler device for subambient temperature analysis (Julabo FT 900); a Mettler STARe thermogravimetric analysis (TGA) system (PerkinElmer Pyris 1, Wellesley, Minneapolis, Minnesota, USA) with simultaneous DSC (TGA/DSC1) measured mass losses on heating.

Finally, the residual humidity, osmolarity and pH of the reconstituted product were measured (see online supplemental material).

Analysis of SFNs internalization by cancer cells

Analyses of SFNs internalization were performed on cancer cell lines and on tumor cells incubated either ex vivo or in vivo with SFNs. Analyses were conducted using either curcumin-loaded SFNs (SFNs-CUR) or SFNs-OVA. In the latter case, an fluorescein isothiocyanate (FITC) rabbit anti-OVA antibody (Abcam, Cambridge, UK) was used as a revealing agent. SFNs internalization was detected by either flow cytometry, using an FACSCanto II flow cytometry (BD) equipped with three lasers (488 nm, 640 nm, 405 nm) using FACSDiva software V.6 (BD), or confocal microscopy, using an Olympus FV500 confocal microscope (Olympus Corporation). Detailed

information on these procedures is provided in the online supplemental material.

Mice

Mice, 7–10 weeks old, female C57BL/6J were purchased from Envigo RMS (San Pietro al Natisone, Udine, Italy) and housed under specific pathogen-free conditions in the animal facility at the Istituto di Ricovero e Cura a Carattere Scientifico (IRCCS) Ospedale Policlinico San Martino, Genoa, Italy. All the procedures were carried out by animal facilities qualified staff according to the guidelines provided in Italian Ministero della Salute D.Lgs 26/2014. The protocol concerning the experiments followed the recommendation and received approval from the Institutional Animal Care and Use Committee (Organizzazione Per il Benessere Animale of IRCCS Ospedale Policlinico San Martino of Genoa) and the National Istituto Superiore di Sanità (protocol # 1000/2020-PR).

Analysis of SFNs internalization by DCs

The analysis of SFNs internalization by DCs was performed by flow cytometry on splenic DCs and DCs present in the TME. Detailed information on these procedures is provided in the online supplemental material.

Adipose adult stromal cells generation

Adipose adult stromal cells were generated as described in detail in the online supplemental material.

MTT assay

Methyl thiazolyl diphenyl-tetrazolium bromide (MTT) assay to assess cell viability was performed as described in the online supplemental material.

Administration of SFNs to tumor-challenged mice

Seven-week-old C57BL/6J female mice were immunized subcutaneously with a suspension of OVA (60 µg) (Merck, Darmstadt, Germania) and CpG 1826 (TIB MolBiol, Genoa, Italy) (30 µg), dissolved in 100 µL saline phosphate buffer without calcium and magnesium (PBS). Two subsequent boosters were administered 15 and 30 days after the first immunization. Ten days after the last booster, B16/F10 mouse melanoma cells or MB49 bladder cancer cells (10^5 cells/mouse) were injected subcutaneously into the mice. Neoplastic nodules were seen at the injection site 7–10 days after tumor cell administration. Mice, randomly distributed among the different treatment and untreated control groups (six mice per group), were administered with SNFs, SFNs-OVA and SFNs-CpG suspended in PBS at 1 mg/mL and sonicated at 59 MHz for 15–30 min at room temperature before subcutaneous injection into the peritumoral area (200 µg per mouse). Each mouse received three nanoparticle injections 1 week apart. Mice were observed daily by researchers who administered the treatments, and blind operators registered tumor sizes. Tumor masses were measured with a caliper at 2–3 days intervals by measuring long and short axes. Volume was calculated according to the formula: tumor volume = ½ (length × width^2) in cm^3. Mice were sacrificed when tumors reached >1 cm^3 or ulceration/bleeding developed.

The experiments aimed at demonstrating the eventual therapeutic effects of SFNs were performed only on the orthotopic B16/F10 melanoma model, more representative of the corresponding human disease than the heterotopic MB49 bladder cancer model, and sized based on our previous experience with the model, following the 3R principle (replacement, reduction and refinement). Tumor measures and laboratory analyses were conducted blind from the treatment group.

Intracellular staining for interferon-γ and interleukin-10 detection

Splenocytes and intratumoral T lymphocytes were purified from OVA hyper-immune C57BL/6J mice challenged with MB49 bladder cancer cells treated or not with SFNs: specimens were minced and passed through a cell strainer to obtain a homogenous cell suspension. Then, lymphocytes were purified by centrifugation on a Ficoll gradient Lympholyte-H Cell Separation Media (Cedarlane, Burlington, Canada). After red blood cell lysis (red blood cell lysing buffer, Merck), splenocytes or tumor-infiltrating lymphocytes were seeded in 96 wells of round-bottomed plates (Corning, Somerville, Massachusetts, USA) in triplicate at 10^6 cells/well in a volume of 100 µL of culture medium (Gibco Life Technologies, Milan, Italy) in the presence or not of OVA (100 µg/mL) overnight. At the end of incubation, the cells were stained with Efluor V450 rat anti-mouse CD3 (Thermo Fisher catalog no 48-0032-82) and PE-Cyanine7 rat anti-mouse CD8 (BD catalog no 552877) antibodies, fixed and permeabilized by BD Cytofix Cytoperm (BD), and incubated with allophycocyanine rat anti-mouse interleukin (IL)-10 (Thermo Fisher catalog no 17-7101-82) and FITC rat anti-mouse interferon (IFN)-γ (Thermo Fisher catalog no 11-7311-82) antibodies. Cells were then analyzed by LSRFortessa X20 flow cytometer (BD).

Cytotoxic assay

B16/F10 melanoma or MB49 bladder cancer cells were incubated overnight with SFNs-OVA or unloaded SFNs as a control in x-vivo medium (Lonza, Basilea, Switzerland) at 37°C in 5% CO_2. Then, the cells were labeled with 5 (6)-carboxyfluorescein diacetate N-succinimidyl ester (CFDA-SE) fluorescent dye (Thermo Fisher Scientific) to track the target cells. Then CFDA-SE labeled cells were seeded in 96 round-bottomed well plates (Corning) at 10^5 cells/well in 200 µL of culture medium. Next, these target cells were incubated overnight with 10^6/well effector T cells sorted (using Dynabeads FlowComp Mouse Pan-T, Thermo Fisher Scientific) from spleen or tumor of OVA hyper-immune mice challenged with either B16/F10 or MB49 cells and treated with SFNs-OVA. Finally, the target cell lysis was measured by adding the viability dye 7-aminoactinomycin D (7-AAD) (BD) at the end of the incubation and expressed as a

percentage of the CFDA-SE+7-AAD+cells. Samples were analyzed using an LSRFortessa X20 flow cytometer (BD).

Proteomic analysis

Sample preparation for liquid chromatography with tandem mass spectrometry analysis

Paraffin-embedded tissue sections from three mice per group of treatment were deparaffinized, proteins were extracted and digested, and the protein mixtures were analyzed by liquid chromatography with tandem mass spectrometry (LC-MS/MS) analysis, as previously reported.[14] The online supplemental material details sample preparation, chromatographic, and MS procedures.

MS/MS data processing

All raw files produced by LC-MS/MS were processed by the SEQUEST HT algorithm in Proteome Discoverer V.2.5 software (Thermo Fisher Scientific, California, USA). Experimental MS/MS spectra were compared with the theoretical mass spectra obtained by in silico digestion of a *Mus musculus* protein database containing 55,315 sequences (www.uniprot.org, accessed on March 1, 2022). The following searching criteria were set: trypsin enzyme, the maximum number of missed cleavages per peptide was set to two, mass tolerances of ±50 ppm for precursor ions and ±0.8 Da for fragment ions. Percolator node was used with a target-decoy strategy to give a final false discovery rate ≤0.01 based on q values, considering a maximum deltaCN of 0.05. Only peptides with peptide lengths of 5–30 amino acids, confidence at 'Medium' level and rank 1 were considered. Protein grouping and strict parsimony principles were applied.

Protein profiles preprocessing, statistical evaluations and quantitative analysis

Peptide spectrum matches (PSMs) of the identified proteins were normalized using a total signal normalization method and compared using a label-free quantification approach as previously reported.[13] Briefly, data matrix dimensionality (MB49 bladder carcinoma, 24 samples×3011 distinct proteins; B16/F10 melanoma, 24 samples×2735 distinct proteins) was reduced by linear discriminant analysis (LDA) and proteins with p value≤0.05 were retained. Pairwise comparisons (CTR vs SFNs-OVA, CTR vs SFNs-CpG) were performed; fold change of proteins selected by LDA was estimated by DAve index[15] comparing the average PSMs (avPSMs). Specifically, positive DAve values indicate proteins upregulated in CTR, whereas negative DAve values indicate proteins upregulated in SFNs-OVA or SFNs-CpG. Finally, differentially expressed proteins (DEPs) selected by LDA were processed by Spearman's rank correlation and hierarchical clustering by applying Ward's method and the Euclidean distance metric. All processing was performed by JMP V.15.2 SAS software.

MB49 bladder carcinoma and B16/F10 melanoma PPI network models

Mus musculus PPI network models were reconstructed starting from all proteins identified in MB49 bladder carcinoma and B16/F10 melanoma using the STRING Cytoscape's application[16]; physical and/or functional interactions were filtered by considering only those 'experiments' or/and 'databases' annotated, with a STRING score ≥0.15 and ≥0.35, respectively. Using the same approach, other two PPI network models were reconstructed starting from DEPs selected for MB49 bladder carcinoma and B16/F10 melanoma, respectively; DEPs were grouped in functional modules by the support of the GO enrichment tool inserted in STRING Cytoscape's Application.[16]

Reconstructed networks were globally analyzed at the topological level by Analyzer application integrated into Cytoscape V.3.8.2.[17] In addition, Centiscape Cytoscape's application[18] calculated betweenness and centroid centralities, and nodes with above-average values were considered PPI hubs.[19] Finally, the statistical significance of all topological results was tested by considering randomized network models[20]; they were reconstructed and analyzed by an in-house R script based on VertexSort (to build random models), igraph (to compute centralities), and ggplot2 (to plot results) libraries; results were visualized in the form of violin plots.

Statistical analysis

Raw data were processed through STATGRAPHICS XVII (StatPoint Technologies, Warrenton, Virginia, USA). A general linear analysis of variance model was generated to evaluate the data. In detail, tumor size data in mice were analyzed considering the treatment and the time as fixed factors and the tumor size as the response variable. The function was then followed by a least significant difference test to estimate the differences between means. Statistical significance was set at $p<0.05$.

RESULTS

Preparation and characterization of SFNs

Injectable formulations containing SFNs, SFNs-OVA and SFNs-CpG were prepared and characterized before in vitro and in vivo testing (figure 1).

Figure 1A shows the morphological analysis of the formulations containing SFNs, SFNs-OVA and SFNs-CpG at three different magnifications (rows a, b and c). As seen at all magnifications, especially row c, the nanoparticles are immersed in a homogeneous matrix of mannitol. At all magnifications, especially rows a and b, the nanoparticles appear round, without apparent aggregates, and with smooth surfaces. Figure 1B shows that the yield percentage was consistently above 70%. The OVA loading percentage was 32.7% for SFNs-OVA. Overall, high encapsulation efficiency for OVA was obtained. For SFNs-CpG, the CpG loading was verified by analyzing their micro-analytical composition. The relative abundance of

A

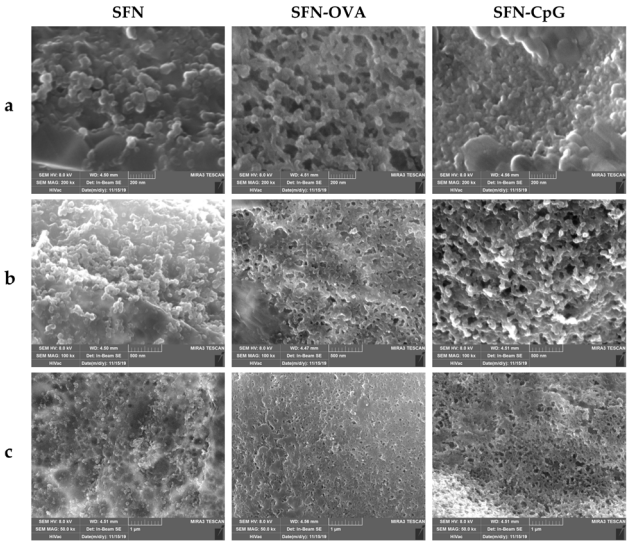

B

Formulation	Yield (%)	Actual drug loading (%)		Assumed drug loading (%)		Encapsulation efficiency (%)	
		OVA	CpG	OVA	CpG	OVA	CpG
SFN	93.6	-	-	-	-	-	-
SFN-OVA	91.7	32.7 ± 0.45	-	33	-	97.0 ± 0.4	-
SFN-CpG	75.2	-	7.36 ± 0.720	-	7	-	-

C

Formulation	Mean diameter ± standard deviation (nm)	Mode ± standard deviation (nm)	d_{10}	d_{50}	d_{90}	Zeta potential (mV)
SFNs	151.7 ± 3.0	103.5 ± 3.6	91.0 ± 1.9	136.6 ± 4.7	219.0 ± 6.4	-17.97
SFN-OVA	141.1 ± 4.6	93.7 ± 3.1	78.9 ± 5.8	111.5 ± 4.1	228.7 ± 19.1	-13.13
SFN-CpG	144.4 ± 4.2	102.7 ± 5.6	84.2 ± 0.9	107.5 ± 4.2	221.9 ± 12.4	-12.97

D

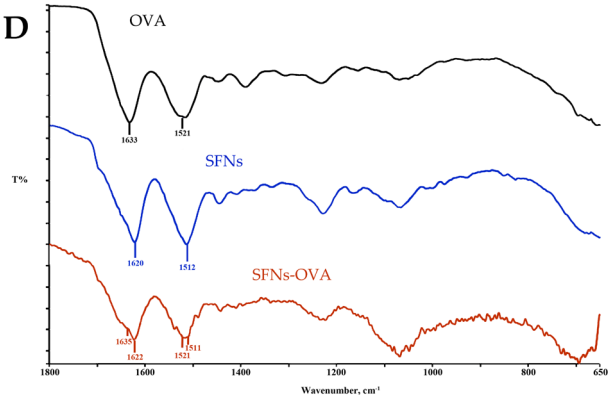

Figure 1 Characterization of SFNs. (A) Morphological investigation by SEM of SFNs, SFNs-OVA and SFNs-CpG at 200 k× (a), 100 k× (b) and 50 k× (c). (B) Yield, encapsulation efficiency and drug loading for the formulations prepared. Data are reported as mean±SD, n=3. (C) Mean diameter, mode, d_{10}, d_{50} and d_{90} for all the samples. Values are reported in nm as mean value±SD, n=5. Z potential is reported in mV. (D) Physico-chemical characterization by IR: enlarged IR spectra between 1800 and 650 cm^{-1} for OVA, SFNs and SFNs-OVA. IR, infrared; OVA, ovalbumin; SFNs, silk fibroin nanoparticles; SEM, scanning electron microscopy.

phosphorus atoms in the mixture was traced back to the percentage amount of CpG, which was 7.36%±0.720 w/w.

All nanoparticle formulations showed a mean diameter of about 150 nm (figure 1C) and a negative surface charge. No significant increase in particle size or change in Z potential was observed after the loading of SFNs with OVA or CpG. The PDI values were lower than 0.3 for all the formulations, confirming that the samples are monodisperse. Overall, the nanoparticle size, morphology and shape are optimal for cancer cells' uptake.[21]

Figure 1D shows the IR spectra between 1800 and 650 cm^{-1}. The protein amide I and II bands are present between 1600–1700 and 1500–1600 cm^{-1}, respectively, the most sensitive region of the IR spectrum for protein secondary structure analysis. In particular, the band at 1633 cm^{-1} in the OVA sample confirmed the presence of

β-sheet structure. Even in the SFNs spectrum, the high content of β-sheet domains is revealed by the characteristic bands in the spectral region of amide I at 1620 cm^{-1} (C=O stretching) and amide II at 1512 cm^{-1} (N–H bending). For SNFs-OVA, the typical bands of amide I and II of the two protein components are distinguishable. This technique did not reveal the presence of CpG in SFNs-CpG as below the sensitivity (data not shown).

The DSC thermal analysis supported the spectroscopic data: all the samples showed a typical profile of an amorphous compound with an endothermic effect around 270°C, associated with a loss of mass in the thermogravimetric curve, linked to sample decomposition (data not shown).

The residual humidity of freeze-dried formulations never exceeded 3%, and the osmolarity value was always between 320 and 350 mOsm/Kg. Moreover, the measured pH value was always in the range of 7.2–7.6.

Internalization of SFNs by cancer cells and DCs

Experiments were conducted to demonstrate that nanoparticles can be effectively up-taken by tumor cells and that this phenomenon is not restricted to a specific cell line or histological type. This first set of experiments was performed using SFNs-CUR, taking advantage of the autofluorescence emitted by curcumin, that makes the test fast and very sensitive. Interestingly, all tested cancer cells showed the capacity to internalize SFNs-CUR although with variable efficiencies, ranging from 40% (LLC1 cells at 1 hour) to 99% (5637 cells at 1 hour) of the total cell population (figure 2, panels A and B). Repeating the experiments using SFNs-OVA, that would have been subsequently administered to mice in the in vivo experiments, we observed again that all tested cell lines internalized the nanoparticles (online supplemental figure S1). Notably, internalization of soluble OVA (i.e., not carried by SFNs) was negligible unless the antigen was mixed with unloaded nanoparticles (a phenomenon likely due to a partial spontaneous OVA absorption on SFNs followed by their internalization by cancer cells). Next, the experiments were repeated on B16/F10 melanoma cells and MB49 bladder cancer cells purified from excised tumors exposed either ex vivo or in vivo to SFNs-OVA. Figure 2C,D show cell internalization of OVA in all experimental conditions.

We also observed that both splenic DCs and DCs present within TME could uptake fibroin nanoparticles (figure 2E and F).

These findings collectively suggest that fibroin nanoparticles are an effective tool to vehicle antigen and adjuvant into both tumor cells and DCs, providing the immunological basis for redirecting effective immune responses within the TME.

In the view of administering SFNs in vivo a relevant issue concerns their eventual direct cytotoxicity. Analysis of cell viability in the above reported tests revealed that SFNs internalization induced a moderate level of cytotoxicity on cancer cells (no more than 20% mortality) but not on healthy DCs, suggesting that nanoparticles may slightly impact on viability of cancer cells but not of healthy cells (online supplemental figure S2A). These data were confirmed by an MTT assay that showed a moderate loss of viability only by cancer cells after 4 hours of exposition to SFNs (again no more than 20% mortality), while viability of one line of adipose tissue-derived stem cells from a healthy donor was not affected (online supplemental figure S2B).

Assessment of immunological and biological effects mediated by SFNs-OVA and SFNs-CpG on TME

Based on the above, we tested the effects of SNFs, SFNs-OVA and SFNs-CpG in vivo. In particular, we addressed two issues: (a) whether SNFs-OVA could redirect into TME and against tumor cells a pre-existing immune response to a non-tumor antigen such as OVA; (b) whether local administrations of either SFNs-OVA or SFNs-CpG were able to induce proteomic changes within TME.

Concerning the first issue, splenic and tumor-infiltrating T lymphocytes were purified from B16/F10 and MB49 cell challenged OVA-hyperimmune mice peritumorally treated with SFNs or SFNs-OVA. Figure 3A and B show that only tumor cells pre-incubated with SFNs-OVA, but not those pre-incubated with unloaded SFNs, were efficiently killed by splenic (14% and 18% of cell lysis for B16/F10 and MB49 cells, respectively) and tumor-infiltrating T cells (19% and 16% of cell lysis for B16F10 and MB49 cells, respectively).

Since in the MB49 tumor we found a richer T-cell tumor infiltrate than in the B16/F10 melanoma, we could also perform experiments testing OVA-specific IFN-γ production by tumor-infiltrating T lymphocytes. Figure 3C shows that IFN-γ-secreting CD4+ and CD8+ OVA-specific T splenocytes were observed in OVA pre-immunized animals, as expected. The frequency of these cells increased in animals treated with SFNs-OVA (figure 3D). When intratumoral T cells were analyzed, IFN-γ-secreting CD4+ and CD8+ OVA-specific T lymphocytes were observed in animals treated with SFNs-OVA but not in untreated ones (figure 3E and F). In the same experiments, the frequency of IL-10-secreting OVA-specific T splenocytes was negligible (figure 3C–3F), suggesting that SFN-OVA immunization privileges the expansion of potential effectors over regulatory T cells.

Concerning the landscape of proteomic variations induced by SFNs-OVA and SFNs-CpG treatments, 2735 and 2463 proteins were identified in B16/F10 melanoma and MB49 bladder cancer, respectively; only 1067 proteins were shared by both models, likely as a result of the different biology of the respective tissues (online supplemental figure S3, datafiles S1 and S2). By comparing the characterized protein profiles, 245 and 332 proteins were found differentially expressed in B16/F10 melanoma and MB49 bladder cancer models, respectively (online supplemental figure S3, datafiles S3 and S4). Of note,

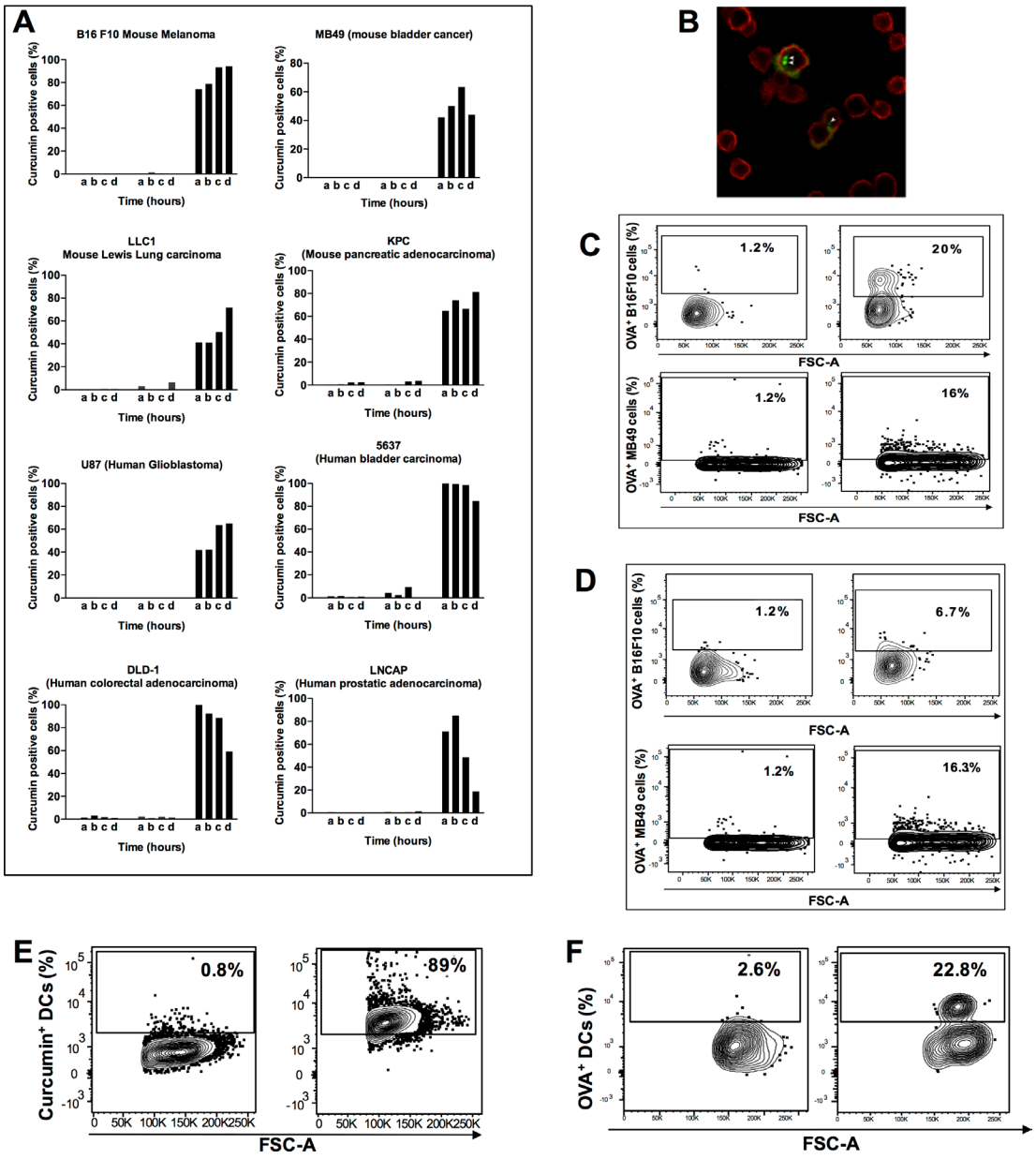

Figure 2 SFNs internalization by cancer cells and DCs. (A) Different mouse or human cancer cell lines were incubated for (a) 1 hour, (b) 2 hours, (c) 4 hours, and (d) 24 hours, alone (left bars) or in the presence of unloaded SFNs (middle bars) or curcumin loaded SFNs (right bars), and evaluated by flow cytometry using a green light-emitting laser; (B) Tumor cells derived from tumors excised from MB49 challenged mice were incubated with curcumin loaded SFNs for 4 hours and evaluated by confocal microscopy (plasma membrane of cells: red signal; curcumin SFNs: green signal). (C) B16/F10 melanoma cells (upper row) and MB49 bladder cancer cells (lower row) purified from an excised tumor were incubated (right panels) or not (left panels) for 4 hours with SFNs-OVA, then fixed and permeabilized before incubation with an anti-OVA FITC labeled mAb and the following cytometric analysis. (D) B16/F10 melanoma cells (upper row) and MB49 bladder cancer cells (lower row) purified from an excised tumor treated peritumorally (right panels) or not (left panels) in vivo with SFNs-OVA were fixed and permeabilized before incubation with an anti-OVA FITC labeled mAb and the following cytometric analysis. (E) Splenic DCs from C57BL/6J mice were incubated (right panel) or not (left panel) for 24 hours with curcumin-loaded SFNs and evaluated by flow cytometry; (F) DCs purified from B16/F10 melanoma tumor excised from SFNs-OVA treated (right panel) or not treated (left panel) mice were fixed and permeabilized before incubation with an anti-OVA FITC labeled mAb and the following cytometric analysis. DCs, dendritic cells; FITC, fluorescein isothiocyanate; FSC-A, forward scatter; mAb, monoclonal antibody; OVA, ovalbumin; SFNs, silk fibroin nanoparticles.

a set of them resulted regulated with the same trend in both models (table 1).

In this context, following SFNs-OVA and SFNs-CpG treatments, we observed downregulation of proteins involved in metastatic progression of cancer cells, such as Hmga1,[22] or erythrocytes (Ank1, Hba-a1, Hbb-b2, Hbb-bs) and blood vessel (Plg) development. On the other hand, proteins involved in endocytosis/major

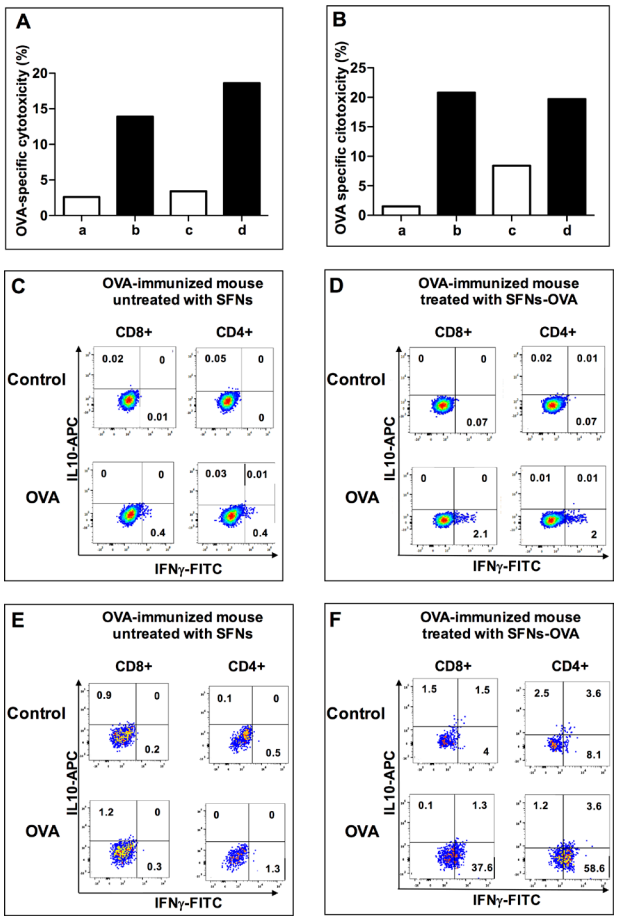

Figure 3 Intratumor expansion of IFN-γ-secreting and cytotoxic OVA-specific T lymphocytes by treatment with SFNs-OVA of tumor-challenged mice pre-immunized against OVA. (A) Cytotoxic activity against B16/F10 melanoma cells pre-exposed to unloaded SFNs (white) or SFNs-OVA (black) by either splenocytes (a–b) or tumor-infiltrating T lymphocytes (c–d) from a representative OVA pre-immunized C57BL/6J mouse challenged with B16-F10 cells and intratumorally treated with SFNs-OVA. (B) Cytotoxic activity against MB49 bladder carcinoma cells pre-exposed to unloaded SFNs (white) or SFNs-OVA (black) by either splenocytes (a–b) or tumor-infiltrating T lymphocytes (c–d) from a representative OVA pre-immunized C57BL/6J mouse challenged with MB49 cells and intratumorally treated with SFNs-OVA. (C) Expansion of OVA-specific T splenocytes in a representative OVA pre-immunized C57BL/6J mouse challenged with MB49 bladder carcinoma cells. Upper row: frequencies of IFN-γ-secreting and IL-10-secreting T splenocytes in a non-antigen stimulated in vitro culture; lower row: frequencies of IFN-γ and IL-10-secreting splenocytes in an OVA stimulated in vitro culture; (D) Expansion of OVA-specific T splenocytes in a representative OVA pre-immunized C57BL/6J mice challenged with MB49 bladder carcinoma cells and intratumorally treated with SFNs-OVA. Upper row: frequencies of IFN-γ-secreting and IL-10-secreting T splenocytes in a non-antigen stimulated in vitro culture; lower row: frequencies of IFN-γ-secreting and IL-10-secreting T splenocytes in an OVA stimulated in vitro culture; (E) Expansion of tumor-infiltrating OVA-specific T lymphocytes in a representative OVA pre-immunized C57BL/6J mouse challenged with MB49bladder carcinoma cells. Upper row: frequencies of IFN-γ-secreting and IL-10-secreting T lymphocytes in a non-antigen stimulated in vitro culture; lower row: frequencies of IFN-γ-secreting and IL-10-secreting T lymphocytes in an OVA stimulated in vitro culture; (F) Expansion of tumor-infiltrating OVA-specific T lymphocytes in a representative OVA pre-immunized C57BL/6J mouse challenged with MB49 bladder carcinoma cells and peritumorally treated with SFNs-OVA. Upper row: frequencies of IFN-γ-secreting and IL-10-secreting T lymphocytes in a non-antigen stimulated in vitro culture; lower row: frequencies of IFN-γ-secreting and IL-10-secreting T lymphocytes in an OVA stimulated in vitro culture. All the experiments were replicated three times. APC, allophycocyanine; FITC, fluorescein isothiocyanate; IFN, interferon; IL, interleukin; OVA, ovalbumin; SFNs, silk fibroin nanoparticles.

histocompatibility complex class II antigen presentation (Capza2, Rab7a, Cltc) and collagen-containing extracellular matrix (Dcn, Lum, Col1a1) were upregulated.

Similarly to their effects on protein expression, SNFs-OVA and SFN-CpG treatments modulated specific functional modules by inducing an analogous expression trend in both models: proteins involved in the immune system function and the vesicle-mediated transport increased their expression, while those related to angiogenesis and T-complex were downregulated (figure 4, online supplemental figures S4–S5).

Indeed, the different biology between the two cancer models could explain some differences and specificities observed following SFNs-OVA and SFNs-CpG treatments, such as downregulation of keratins, potential prognostic markers in melanoma,[23] and SERPINs,[24] that appeared

Table 1 Differentially expressed proteins with the same expression trend in both models

	B16/F10melanoma		MB49 bladder cancer	
Gene name	CTR vs SFNs-OVA*	CTR vs SFNs-CpG	CTR vs SFNs-OVA	CTR vs SFNs-CpG
Ank1	2.0	2.0	1.6	2.0
Ero1a	1.1	2.0	0.2	0.4
Hba-a1	1.1	1.2	1.0	0.7
Hbb-b2	0.9	0.8	0.8	1.3
Hbbs	1.5	1.5	0.7	1.2
Hmga1	2.0	2.0	2.0	2.0
Myadm	2.0	2.0	2.0	1.6
Plec	1.4	0.9	0.4	1.2
Plg	1.5	0.8	1.0	0.9
Snrpf	2.0	1.4	2.0	2.0
Stom	2.0	2.0	2.0	2.0
Aldh2	−0.4	−0.8	−1.0	−1.5
Capza2	−1.4	−1.6	−0.4	−0.8
Cltc	−0.8	−0.6	−0.5	−0.5
Col1a1	−1.1	−1.0	−0.9	−1.3
Dcn	−1.4	−1.4	−2.0	−2.0
Lum	−2.0	−2.0	−2.0	−2.0
Msn	−0.4	−0.7	−1.0	−1.3
Rab7a	−1.0	−1.4	−1.0	−0.3
Rps16	−0.9	−0.7	−0.5	−0.2

*For each pairwise comparison (CTR vs SFNs-OVA; CTR vs SFNs-CpG) DAve index is shown; positive DAve values indicate proteins upregulated in CTR (downregulated in SFNs treatments), while negative DAve values indicate proteins upregulated following SFNs treatments (downregulated in CTR).
CTR, control; OVA, ovalbumin; SFN, silk fibroin nanoparticle.

more consistent in the B16/F10 melanoma model than in the MB49 one (online supplemental figure S6).

Comparing the effects differentially mediated by SFNs-OVA and SFNs-CpG treatments, SFNs-OVA were found to be more effective in reducing angiogenesis, while SFNs-CpG in reducing keratins expression and in upregulating proteins involved in immune system activity (online supplemental figures S4–S6).

Hub proteins as key players of the proteome modulation mediated by SFNs-OVA and SFNs-CpG treatments

Interesting indications that support the efficacy of SFNs-OVA and SFNs-CpG treatments emerged from the topological analysis of PPI network models (online supplemental figure S7).

In this context, concerning the B16/F10 melanoma model, both Akt1 and Pik3r2, the best-ranked hubs in untreated tumors, were not identified in any B16/F10 samples treated with SFNs-OVA and SFNs-CpG (Data file S5), likely sign of tumor suppressive effect based on the well-known protumoral effects of both pathways reported in melanoma and other cancers.[25 26] Conversely, Itgb2, whose expression was reported to correlate with the infiltration of all types of immune cells,[27 28] potentially predisposing to improved effectiveness of immunotherapy and improved overall survival, was the best-ranked hub in all B16/F10 samples treated with SFNs-OVA and SFNs-CpG (Data online supplemental file 5). Fau was another interesting hub found in all B16/F10 samples treated with SFNs-OVA and SFNs-CpG since it has been proposed as a candidate tumor suppressor protein acting by regulation of apoptosis in human cells.[29]

Concerning the MB49 bladder cancer model, we found high mobility group protein HMGI-C (Hmga2) as the best-ranked hub protein (Data file S6); this protein, which was not identified in any MB49 samples treated with SFNs-OVA and SFNs-CpG, has been widely associated with cancer progression,[30] also in the bladder,[31] and is specifically targeted to inhibits bladder cancer metastasis.[32 33] On the opposite, cAMP-dependent protein kinase (PKA) catalytic subunit beta (Prkacb), a catalytic subunit of cAMP-dependent PKA that regulates numerous fundamental biological processes such as metabolism, development, memory, and immune response, resulted the best hub of all MB49 samples treated with SFNs-OVA and SFNs-CpG and of B16/F10 melanoma samples treated with SFNs-OVA (Data files S5 and S6). This is of relevance since Prkacb gene encodes several splice variants, including Cβ2, which is enriched in T cells, B cells and natural killer cells,[34] and its increased expression is associated with a favorable prognosis in different cancers.[35] The best-ranked hubs following treatment with SFNs-OVA in MB49 samples were cytotoxic granule-associated RNA binding protein TIA1 (Tia1) and nuclear factor of kappa light polypeptide gene enhancer in B cells 1 (Nfkb1). Noteworthy, Tia1 has been described as an important tumor suppressor molecule,[29] and other authors speculated that CD8/Tia1+infiltrating TME confer superior survival to patients with localized osteosarcoma.[36] Also of note, the knockout of Nfkb1, an important regulator of NF-κB activity in vivo, has been associated in mouse models with increased inflammation and susceptibility to certain forms of DNA damage, leading to cancer and a rapid aging phenotype.[37]

Therapeutic efficacy of the different SNFs formulations

OVA hyperimmune, B16/F10 melanoma-challenged C57BL/6J mice were untreated or treated peritumorally with either unloaded SFNs, SFNs-OVA, SFNs-CpG or the combination of SFNs-OVA plus SFNs-CpG. Both treatments with SFNs-OVA and SFNs-CpG significantly slowed tumor growth compared with the last two control groups of mice (figure 5). When B16/F10 melanoma-challenged mice were treated with a combination of SNFs-OVA and SFNs-CpG, tumor growth was significantly reduced compared with control mice and mice treated with either SFNs-OVA alone or SFNs-CpG alone (figure 5), showing a remarkable additive effect likely due to the association of their mechanisms of action. Proteomic analyses were performed on tumor specimens from mice treated with the combination of SFNs-OVA and SFNs-CpG to assess this possibility (figure 6).

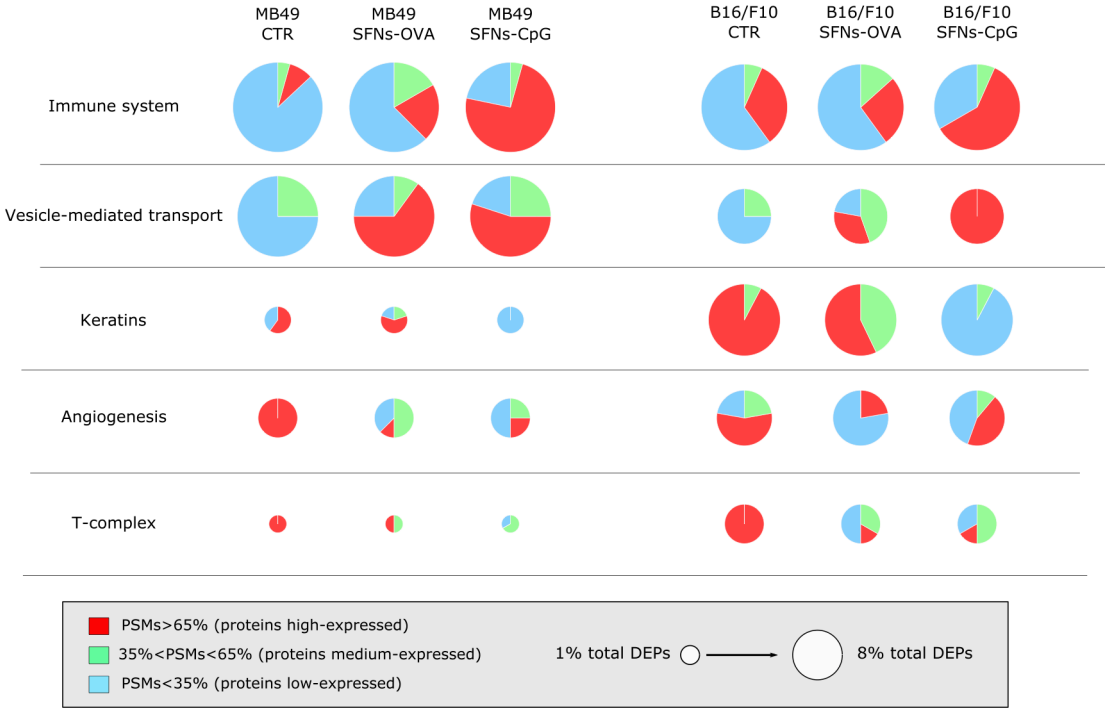

Figure 4 Proteomic and systems biology outcomes of SFNs administration at the tumor site. The analyses evidence the functional modules affected by SNFs-OVA and SFN-CpG treatments in both MB49 bladder cancer and B16/F10 melanoma models. Red, green and blue color codes indicate the percentage of proteins with high-, medium- and low expression, respectively, based on a PSMs-based label-free quantification. The pie chart size is proportional to the number of DEPs per module. CTR, control; DEP, differentially expressed protein; OVA, ovalbumin; SFNs, silk fibroin nanoparticles.

Correlation among DEP profiles was observed, indicating a consistent proteome remodeling and a synergic effect of SFNs-OVA and SFNs-CpG treatment (figure 6). This mainly appeared evident for keratins, complement and coagulation cascades, angiogenesis, SERPINs and erythrocyte-related proteins, which were mainly downregulated following the action of both SFNs-OVA and SFNs-CpG. Of note, keratins' downregulation appeared

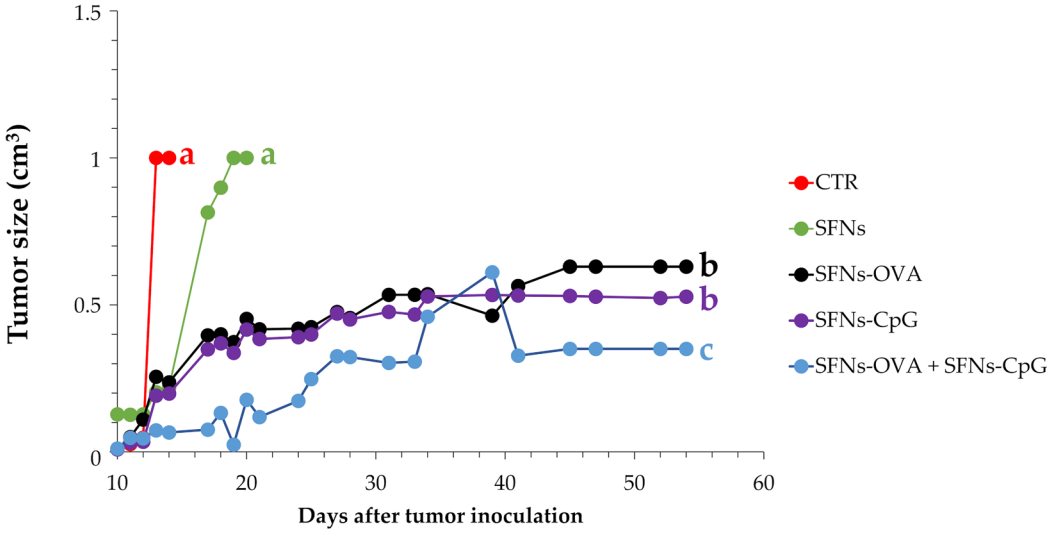

Figure 5 Effects of SFNs-OVA, SFNs-CpG, and their combination on B16/F10 melanoma growth. Tumor size is shown as a function of time (days after tumor inoculation) and treatment with or without SFNs. Mice (six per group) were sacrificed when the tumor reached 1 cm^3. Data are reported as mean values, and error bars were not displayed on the plots for clarity, but uncertainties were within ~15%. Different letters indicate a significant difference between the means of the corresponding groups: in particular, a p value<0.00001 was found in the comparisons a versus b and a versus c, while a p value<0.001 was observed in the comparison b versus c. The same letters indicate no significant differences (p>0.05) (multifactor analysis of variance, and Fisher's least significant difference, least significant difference, to discriminate among the means). CTR, control; OVA, ovalbumin; SFNs, silk fibroin nanoparticles.

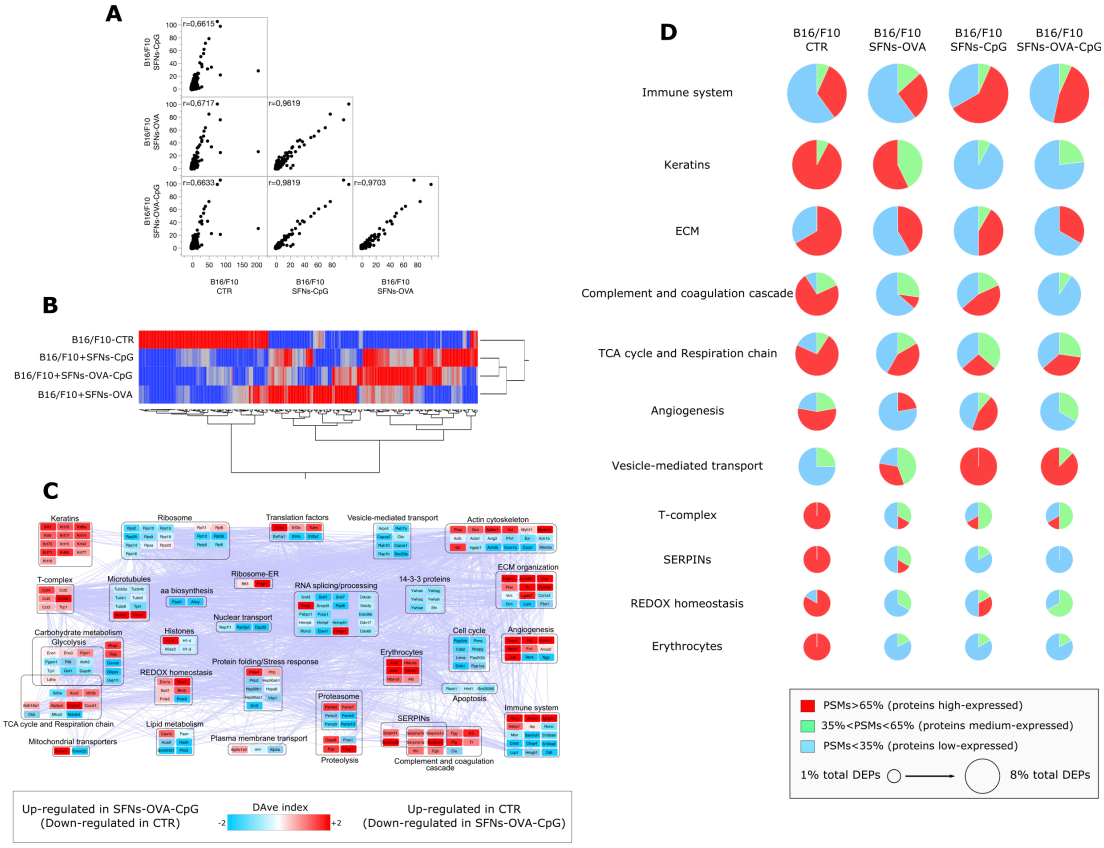

Figure 6 Proteome and functional modules characterized by nLC-hrMS/MS analysis of tissues from the B16/F10 melanoma model. (A) Spearman's correlation and hierarchical clustering (B) among profiles of DEPs. (C) PPI network model reconstructed by Cytoscape's STRING application starting from proteins differentially expressed by comparing B16/F10 melanoma model untreated (CTR) and treated with SFNs-OVA plus SFNs-CpG. Proteins were grouped in functional modules. The red color code (positive DAve values) indicates proteins upregulated in CTR (vs SFNs-OVA plus SFNs-CpG samples), while the blue color code (negative DAve values) indicates proteins upregulated in SFNs-OVA plus SFNs-CpG samples (vs CTR). (D) Functional modules most affected by SNFs treatments in B16/F10 melanoma model. Red, green and blue color codes indicate the percentage of proteins with high expression, medium expression and low expression, respectively, based on a PSMs-based label-free quantification. The pie chart size is proportional to the number of DEPs per module. CTR, control; DEP, differentially expressed protein; ECM, extracellular matrix; OVA, ovalbumin; PSMs, peptide spectrum matches; SFNs, silk fibroin nanoparticles; TCA, tricarboxylic acid cycle.

mainly mediated by the presence of CpG, while OVA mainly affected the downregulation of the complement and coagulation cascades, suggesting not only an additive mechanism of action but complementary as well.

DISCUSSION

In this study, we explored an innovative active immunotherapy approach aimed at redirecting a previously consolidated immune response toward the tumor against a re-call antigen. In our system, a non-tumor-associated antigen was delivered within tumor cells using SFNs. SF has been selected as the material to nanoencapsulate antigen and adjuvant because it is biocompatible, it provides mechanical durability, and its enzyme-mediated degradation supports the sustained intracellular release after nanoparticle uptake by cancer cells.[21] Clearly, based on the use of SFNs, our system provides a safety profile that escapes the concerns related to administering live pathogens to potentially immune-compromised patients, which has been recently reported.[38] Also, following administration in mice, the lack of inflammatory signs at peripheral tissues seems to rule out the risks related to the onset of inflammatory/autoimmune manifestations; this is probably linked to the fact that, in our model, SFNs are administered at the tumor site, and both tumor and DCs exert a preferential uptake. In this regard, the selective uptake of SFNs by tumors may be further refined through the functionalization of the nanoparticle surface with ligands able to provide active targeting, and many examples in the literature exploited the large amounts of available amino and carboxyl groups in fibroin peptides to link oligonucleotides or peptides.[39–44] This may also avoid the onset of an autoimmune response when the nanoparticles are uptaken by healthy instead of tumor cells.

Our data also showed that our approach effectively redirected immunity against a re-call antigen toward

the tumor, involving in this process both innate and adoptive harms of the immune response (in particular, DCs, which were shown to efficiently uptake SFNs, and T cells, respectively). Concerning DCs, their involvement is important since these cells orchestrate innate and adaptive immune responses, so their function is crucial for effective anticancer immunity.[45] Concerning T cells, both CD4+ and CD8+ IFN-γ-secreting/cytotoxic T cells were detected among tumor-infiltrating lymphocytes of SFNs-OVA treated mice, specifically demonstrating the efficiency of our 'Trojan horse' strategy in redirecting the anti-OVA immune response against tumor cells.

The proteomic analyses of tumors treated with SFNs, and their evaluation at a holistic level by network models, allowed us to appreciate the involvement of not strictly immune-mediated mechanisms among the effects of the treatments.

Indeed, our data envisage the possibility of translating into clinics this 'Trojan-horse', immune response-centered strategy, that is, adopting, as immunogens, antigens of the compulsory vaccines recommended by the international health institutes for the prevention of infectious diseases. The advantage of this 'Trojan-horse' approach would be that each single patient with cancer, independently from the tumor's histological nature, could have already at play the appropriate immunological background to be treated. Hence, this approach would recapitulate the essence of personalized medicine with the need for universality. The 'Trojan-horse' approach could also synergize well with immune checkpoint inhibitors, favoring the unleashing of T cells effector activities. Finally, based on the continuous improvement of technologies for local site delivery of immunotherapies,[46] our innovative strategy could find a role in the treatment with eradication purpose of non-metastatic tumors, such as glioblastoma, as well as in palliative therapy of all surgically unresectable tumor masses. However, to ensure clinical success, many challenges in the translation from bench to bedside still must be addressed for SFNs, ranging from the technological and Good Manufacturing Practice large-scale manufacturing challenges, including quality control and batch release requirements, to the biological ones, including biocompatibility, biodegradability and safety, as we recently discussed in detail.[47]

Author affiliations
[1]Department of Pharmaceutical Sciences, University of Piemonte Orientale, Novara, Piemonte, Italy
[2]Department of Internal Medicine and Centre of Excellence for Biomedical Research, University of Genoa, Genova, Liguria, Italy
[3]Department of Drug Sciences, University of Pavia, Pavia, Lombardia, Italy
[4]PharmaExceed S.r.l, Pavia, Lombardia, Italy
[5]Institute for Biomedical Technologies, ITB CNR, Segrate, Lombardia, Italy
[6]Anatomic Pathology Unit, IRCCS Ospedale Policlinico San Martino, Genova, Liguria, Italy
[7]Department of Surgical and Integrated Diagnostic Sciences, University of Genoa, Genova, Liguria, Italy
[8]Biotherapy Unit, IRCCS Ospedale Policlinico San Martino, Genova, Liguria, Italy

Acknowledgements The authors thank Dr Sara Tengattini from University of Pavia, Department of Drug Sciences for OVA quantitative analysis, and Dr Ilaria Giuseppina Tredici from the Arvedi Laboratory, CISRiC (Centro Interdipartimentale di Studi e Ricerche per la Conservazione del Patrimonio Culturale), Pavia, Italy for the scanning electron microscopy and energy dispersive spectrometry analyses. Also, The authors also thank Professor Lorenzo Moretta and Professor Paola de Candia for their precious suggestions and comments on the manuscript.

Contributors Guarantor: GF. Conceptualization: GF, MLT, DDS. Methodology: EB, FF, TA, SP, PM, RR, GP, LM, DF, GF. Investigation: EB, FF, TA, SP, PM, RR, GP, LM, MG, GIA, MM, DF. Visualization: GF, MLT, DDS, DF, FF, LM. Funding acquisition: GF, MLT, DDS, PM. Project administration: GF, MLT. Supervision: GF, MLT, DDS. Writing—original draft: GF, MLT, DDS. Writing—review and editing: GF, MLT, DDS, FF, DF, EB.

Funding This research was funded by grants from: Ministero della Salute, Progetto 5M-2019-2366468 – 5 per mille, 'Generazione di organoidi tumorali da neoplasia solide ed ematologiche'; PON ELIXIR CNR-BiOMICS (PIR01_00017), Elixir Implementation Study Proteomics (2019–2021 and 2021–2023) and Italian Ministry of Health (RF2019-12370396); Interreg V-A Italy-Switzerland 2014–2020—ATEx—Advanced Therapies Experiences (Project ID 637541).

Competing interests Data presented in this manuscript pertain to the Italian Patent Application N. 102019000008658 'Immunizzazione antitumorale mediata da nanoparticelle e basata su un'immunità preesistente' filed on June 11, 2019, granted on April 21, 2021, and the international patent application PCT/IB2020/055456 'Nanoparticles for use in the redirection against the tumour of a non-tumour-specific immune response, based on a pre-existing immunity', Publication number WO/2020/250153, filed on June 10, 2020.The authors who are co-inventors in these patents are EB, FF, DF, SP, MLT and GF.

Patient consent for publication Not applicable.

Ethics approval Not applicable.

Provenance and peer review Not commissioned; externally peer reviewed.

Data availability statement All data relevant to the study are included in the article or uploaded as supplementary information. All data are available in the main text or the Supplemental materials.

ORCID iDs
Elia Bari http://orcid.org/0000-0003-0241-0620
Giuseppina Iliana Astone http://orcid.org/0000-0003-4206-3491
Maria Luisa Torre http://orcid.org/0000-0001-8062-6836
Gilberto Filaci http://orcid.org/0000-0001-6445-8414

REFERENCES

1 Rosenberg SA, Yang JC, Restifo NP. Cancer immunotherapy: moving beyond current vaccines. *Nat Med* 2004;10:909–15.
2 Small EJ, Schellhammer PF, Higano CS, *et al*. Placebo-Controlled phase III trial of immunologic therapy with sipuleucel-T (APC8015) in patients with metastatic, asymptomatic hormone refractory prostate cancer. *J Clin Oncol* 2006;24:3089–94.
3 Saxena M, van der Burg SH, Melief CJM, *et al*. Therapeutic cancer vaccines. *Nat Rev Cancer* 2021;21:360–78.
4 Lee C-H, Yelensky R, Jooss K, *et al*. Update on tumor neoantigens and their utility: why it is good to be different. *Trends Immunol* 2018;39:536–48.
5 Rammensee H-G, Singh-Jasuja H. Hla ligandome tumor antigen discovery for personalized vaccine approach. *Expert Rev Vaccines* 2013;12:1211–7.

6 Januszkiewicz-Lewandowska D, Gowin E, Bocian J, *et al*. Vaccine-Derived immunity in children with Cancer-Analysis of anti-tetanus and Anti-Diphtheria antibodies changes after completion of antineoplastic therapy. *Pediatr Blood Cancer* 2015;62:2108–13.
7 Sau S, Alsaab HO, Bhise K, *et al*. Multifunctional nanoparticles for cancer immunotherapy: a groundbreaking approach for reprogramming malfunctioned tumor environment. *J Control Release* 2018;274:24–34.
8 Gao S, Yang D, Fang Y, *et al*. Engineering nanoparticles for targeted remodeling of the tumor microenvironment to improve cancer immunotherapy. *Theranostics* 2019;9:126–51.
9 Nasirmoghadas P, Mousakhani A, Behzad F, *et al*. Nanoparticles in cancer immunotherapies: an innovative strategy. *Biotechnol Prog* 2021;37:e3070.
10 Perteghella S, Crivelli B, Catenacci L, *et al*. Stem cell-extracellular vesicles as drug delivery systems: new frontiers for silk/curcumin nanoparticles. *Int J Pharm* 2017;520:86–97.
11 Crivelli B, Perteghella S, Bari E. Silk nanoparticles: from inert supports to bioactive natural carriers for drug delivery. *Soft Matter* 2017.
12 Crivelli B, Bari E, Perteghella S, *et al*. Silk fibroin nanoparticles for celecoxib and curcumin delivery: ROS-scavenging and anti-inflammatory activities in an in vitro model of osteoarthritis. *Eur J Pharm Biopharm* 2019;137:37–45.
13 Palma C, La Rocca C, Gigantino V, *et al*. Caloric restriction promotes immunometabolic reprogramming leading to protection from tuberculosis. *Cell Metab* 2021;33:300–18.
14 Bari E, Di Silvestre D, Mastracci L. GMP-compliant sponge-like dressing containing MSC lyo-secretome: proteomic network of healing in a murine wound model. *Eur J Pharm Biopharma* 2020.
15 Di Silvestre D, Brambilla F, Mauri PL. Multidimensional protein identification technology for direct-tissue proteomics of heart. *Methods Mol Biol* 2013;1005:25–38.
16 Doncheva NT, Morris JH, Gorodkin J, *et al*. Cytoscape StringApp: network analysis and visualization of proteomics data. *J Proteome Res* 2019;18:623–32.
17 Su G, Morris JH, Demchak B, *et al*. Biological network exploration with Cytoscape 3. *Curr Protoc Bioinformatics* 2014;47:11–24.
18 Scardoni G, Tosadori G, Faizan M, *et al*. Biological network analysis with CentiScaPe: centralities and experimental dataset integration. *F1000Res* 2014;3:139.
19 Burrello J, Tetti M, Forestiero V, *et al*. Characterization of circulating extracellular vesicle surface antigens in patients with primary aldosteronism. *Hypertension* 2021;78:726–37.
20 Tosadori G, Bestvina I, Spoto F, *et al*. Creating, generating and comparing random network models with NetworkRandomizer. *F1000Res* 2016;5:2524.
21 Donahue ND, Acar H, Wilhelm S. Concepts of nanoparticle cellular uptake, intracellular trafficking, and kinetics in nanomedicine. *Adv Drug Deliv Rev* 2019;143:68–96.
22 Wang Y, Hu L, Zheng Y, *et al*. Hmga1 in cancer: cancer classification by location. *J Cell Mol Med* 2019;23:2293–302.
23 Han W, Hu C, Fan Z-J, *et al*. Transcript levels of keratin 1/5/6/14/15/16/17 as potential prognostic indicators in melanoma patients. *Sci Rep* 2021;11:1023.
24 Lorenz N, Loef EJ, Verdon DJ, *et al*. Human T cell activation induces synaptic translocation and alters expression of the serine protease inhibitor neuroserpin and its target protease. *J Leukoc Biol* 2015;97:699–710.
25 Kircher DA, Trombetti KA, Silvis MR, *et al*. AKT1^{E17K} Activates Focal Adhesion Kinase and Promotes Melanoma Brain Metastasis. *Mol Cancer Res* 2019;17:1787–800.
26 Liu J, Zhong F, Cao L, *et al*. 7-Dehydrocholesterol suppresses melanoma cell proliferation and invasion via Akt1/NF-κB signaling. *Oncol Lett* 2020;20:1.
27 Nurzat Y, Su W, Min P, *et al*. Identification of therapeutic targets and prognostic biomarkers among integrin subunits in the skin cutaneous melanoma microenvironment. *Front Oncol* 2021;11:751875.
28 Kwak M, Erdag G, Leick KM, Leick LaRoche KM, *et al*. Associations of immune cell homing gene signatures and infiltrates of lymphocyte subsets in human melanomas: discordance with CD163+ myeloid cell infiltrates. *J Transl Med* 2021;19:371–23.
29 Liu Y, Liu R, Yang F, *et al*. miR-19A promotes colorectal cancer proliferation and migration by targeting TIA1. *Mol Cancer* 2017;16:53.
30 Mansoori B, Mohammadi A, Ditzel HJ, *et al*. Hmga2 as a critical regulator in cancer development. *Genes* 2021;12:269.
31 Yang GL, Zhang LH, Bo JJ, *et al*. Overexpression of HMGA2 in bladder cancer and its association with clinicopathologic features and prognosis HMGA2 as a prognostic marker of bladder cancer. *Eur J Surg Oncol* 2011;37:265–71.
32 Chen Z, Li Q, Wang S, *et al*. miR-485-5p inhibits bladder cancer metastasis by targeting HMGA2. *Int J Mol Med* 2015;36:1136–42.
33 Shi Z, Li X, Wu D, *et al*. Silencing of HMGA2 suppresses cellular proliferation, migration, invasion, and epithelial-mesenchymal transition in bladder cancer. *Tumour Biol* 2016;37:7515–23.
34 Moen LV, Sener Z, Volchenkov R, *et al*. Ablation of the Cβ2 subunit of PKA in immune cells leads to increased susceptibility to systemic inflammation in mice. *Eur J Immunol* 2017;47:1880–9.
35 Tang J, Luo Y, Wu G. A glycolysis-related gene expression signature in predicting recurrence of breast cancer. *Aging* 2020;12:24983–94.
36 Palmerini E, Agostinelli C, Picci P, *et al*. Tumoral immune-infiltrate (IF), PD-L1 expression and role of CD8/TIA-1 lymphocytes in localized osteosarcoma patients treated within protocol ISG-OS1. *Oncotarget* 2017;8:111836–46.
37 Cartwright T, Perkins ND, L Wilson C. Nfkb1: a suppressor of inflammation, ageing and cancer. *Febs J* 2016;283:1812–22.
38 Selvanesan BC, Chandra D, Quispe-Tintaya W, *et al*. *Listeria* delivers tetanus toxoid protein to pancreatic tumors and induces cancer cell death in mice. *Sci Transl Med* 2022;14:eabc1600.
39 Mao B, Liu C, Zheng W, *et al*. Cyclic cRGDfk peptide and chlorin E6 functionalized silk fibroin nanoparticles for targeted drug delivery and photodynamic therapy. *Biomaterials* 2018;161:306–20.
40 Mottaghitalab F, Kiani M, Farokhi M, *et al*. Targeted delivery system based on Gemcitabine-Loaded silk fibroin nanoparticles for lung cancer therapy. *ACS Appl Mater Interfaces* 2017;9:31600–11.
41 Bian X, Wu P, Sha H, *et al*. Anti-EGFR-iRGD recombinant protein conjugated silk fibroin nanoparticles for enhanced tumor targeting and antitumor efficiency. *Onco Targets Ther* 2016;9:3153–62.
42 Gou S, Huang Y, Wan Y, *et al*. Multi-bioresponsive silk fibroin-based nanoparticles with on-demand cytoplasmic drug release capacity for CD44-targeted alleviation of ulcerative colitis. *Biomaterials* 2019;212:39–54.
43 Rodriguez-Nogales A, Algieri F, De Matteis L, *et al*. Intestinal anti-inflammatory effects of RGD-functionalized silk fibroin nanoparticles in trinitrobenzenesulfonic acid-induced experimental colitis in rats. *Int J Nanomedicine* 2016;11:5945–58.
44 Bari E, Serra M, Paolillo M, *et al*. Silk fibroin nanoparticle functionalization with Arg-Gly-Asp cyclopentapeptide promotes active targeting for tumor site-specific delivery. *Cancers* 2021;13:1185.
45 Plesca I, Müller L, Böttcher JP, *et al*. Tumor-Associated human dendritic cell subsets: phenotype, functional orientation, and clinical relevance. *Eur J Immunol* 2022;52:1750–8.
46 Wang J, Zhang Y, Pi J, *et al*. Localized delivery of immunotherapeutics: a rising trend in the field. *J Control Release* 2021;340:149–67.
47 Bari E. From bench to bedside: the long way towards GMP scale-up, preclinical and clinical trials for Silk-based drug delivery systems.. In: *Silk-Based drug delivery systems*, 2021: 179–204.